Potential and Optimal Target Fixating Control of the Human Head/Eye Complex

Indika Bandara Wijayasinghe, Eugenio Aulisa, Ulrich Büttner, Bijoy Kumar Ghosh, Stefan Glasauer, and Olympia Kremmyda

***Abstract*— The human head and eye rotate in coordination to rapidly project images of stationary targets from the visual space. Once a target is fixated, the head/eye complex maintains stability of the image, even while the head continues to move toward the target. The orientation of the head is constrained by Donders' law, whereas the final orientation of the eye satisfies Listing's constraint with respect to the final orientation of the head. The eye is rotated opposite to the movement of the head to compensate and maintain image stability. Using dynamic modeling, this brief investigates the underlying target fixating control mechanisms behind the head and eye movements. Finally, model output trajectories of the head and eye are compared with the corresponding experimentally observed trajectories.**

***Index Terms*— Donders' law, eye movement, head movement, Listing's law, optimal control, potential control, target fixation.**

I. Introduction

MODELING and control of the human eye have been of interest since mid nineteenth century with notable studies conducted in [1]–[3]. It has been observed [2] that, when the head coordinates are fixed, the oculomotor system chooses just one angle of ocular torsion for any one gaze direction. In particular, the axes of rotations of the eye, away from the primary gaze direction, always lie on a fixed plane called the Listing's plane. It turns out that the head movements are similarly constrained by the so called Donders' law [4]. Human head is mechanically able to rotate torsionally, but normally adopts to just one torsional angle for any one facing direction [5]–[7]. A geometric consequence of the Donders' law is that the 3-D vectors that represent the rotational vectors[1] of the head are not spread out in a 3-D volume, but instead fall in a single 2-D surface known as the Donders' surface.

When the head and the eye are both allowed to move freely, the situation is a bit more complicated [8]. In an attempt to fixate on a target, eye violates the Listing's constraint. In doing so, the eye saccades and may move on to an eccentric position, ahead of the head. The eye does not stay in that position, but rotates backward, while the head moves forward, satisfying Donders' constraint, toward the target. As the eye recovers from its initial surge, invariance of the image on the retina is guaranteed by the eye controller. In other words, forward head movements are compensated by a backward movement of the eye.[2] In addition, it has been observed that, in the steady state, when both the head and the eye have momentarily reached a point of immobility, the ocular torsion is once again close to zero. It indicates that at the point of immobility, Listing's constraint is satisfied.

Using a dynamic model for the head and the eye movement,[3] together with potential and optimal control methods [10], we simulate the head and the eye movement control systems as they move to acquire a point target in space (see [11], [12] for additional recent work on optimal control of eye-head movements). During the process of target acquisition, initially the head moves in the same direction as the eye, and both toward the target. In this brief, no *a priori* conjecture is made regarding the head trajectory and the boundary constraints the head satisfy, except that the head orientations satisfy Donders' constraint throughout the entire trajectory. The eye moves faster than the head and fixates on the target, choosing non-zero values of ocular torsion during its movement. The head continues to move past the time when the target has been fixated. During the post acquisition time, the eye backtracks the forward head movement (see footnote 2), until the head and the eye, both comes to rest at zero ocular torsion. This brief describes results from three different simulation scenarios on head and eye control.

Simulation 1: We start with trajectories of the human head and eye constructed out of experimentally observed data. Using a dynamic model of human head and eye, we track these observed trajectories using an optimal tracking strategy.

Simulation 2: For each of the experimentally observed head trajectories, considered in Simulation 1, a suitable boundary constraint on the head is computed.[4] Head trajectories are now simulated by requiring that the model head starts and ends at the prescribed boundary points at a prescribed fixed

Manuscript received January 11, 2014; accepted May 20, 2014. Manuscript received in final form June 22, 2014. This work was supported by the National Science Foundation under Grant 1029178. Recommended by Associate Editor M. Guay.

I. B. Wijayasinghe is with the Department of Mathematics and Statistics, Sam Houston State University, Huntsville, TX 77340 USA (e-mail: indika.wijayasinghe@ttu.edu).

E. Aulisa and B. K. Ghosh are with the Department of Mathematics and Statistics, Texas Tech University, Lubbock, TX 79409 USA (e-mail: eugenio.aulisa@ttu.edu; bijoy.ghosh@ttu.edu).

U. Büttner and S. Glasauer are with the Integrated Research and Treatment Center for Vertigo IFB-LMU, University Clinic Munich, Munich 80337, Germany, and also with the Center of Sensorimotor Research, Ludwig-Maximilians University, Munich 80539, Germany (e-mail: ulrich.buettner@med.uni-muenchen.de; s.glasauer@lrz.uni-muenchen.de).

O. Kremmyda is with the Department of Neurology, Ludwig-Maximilians University, Munich 80539, Germany (e-mail: olympia.kremmyda@med.uni-muenchen.de).

Color versions of one or more of the figures in this paper are available online at http://ieeexplore.ieee.org.

Digital Object Identifier 10.1109/TCST.2014.2335115

[1] These are the axes of rotation suitably scaled. See Section II of this brief for a precise definition.

[2] We use the convention that forward head movement is a head movement toward the target. Backward eye movement, on the other hand, is a movement opposite to the moving direction of the head.

[3] See [9] for a geometric introduction to the eye and head movement dynamics.

[4] At the boundary, the model head is constrained to be on the Donders' surface closest to the actual orientation of the subject head.

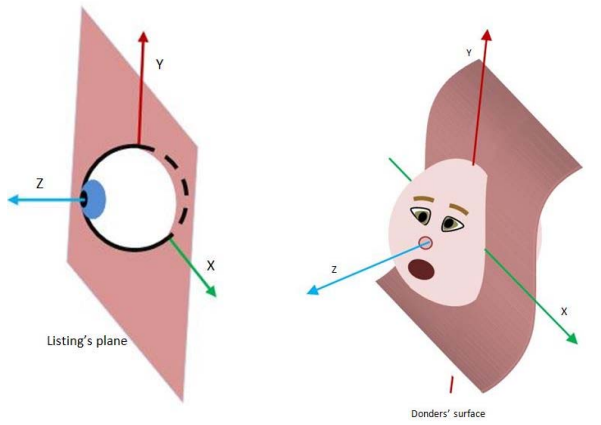

(a) (b)

Fig. 1. Eye and head coordinate systems shown here are from [9]. The two coordinates are centered at the center of the eye and the head, respectively. In addition, during our study of the eye/head complex, the centers of the eye and the head are assumed to be at the same point. (a) Eye coordinate system, with respect to the moving head, showing the Listing's plane. (b) Head coordinate system, with respect to fixed torso, showing the Donders' surface.

time,[5] while the control input to the head movement dynamics minimizes a cost function. Eye trajectories are simulated by requiring that the model eye tracks a suitably computed tracking signal.[6]

Simulation 3: Boundary constraints on the head are computed as described in Simulation 2. We construct a potential function that has its minimum at the terminal boundary point. A potential control is applied to the model head together with an additional damping term [10], that rotates the head toward the terminal boundary point. Eye trajectories are simulated by requiring that the model eye tracks a computed tracking signal (see footnote 6). The tracking control is derived by introducing a potential and a damping function as well.

This brief illustrates the role of an eye tracking signal that the eye needs to track to keep image of the target stationary, in spite of head movement, once the eye has fixated on the target. Using experimentally observed data, we confirm the role of the proposed tracking signal. The tracking controllers are synthesized using optimal and potential control methods. This brief compares the simulated head/eye trajectories with the trajectories constructed from the collected data. In addition, this brief compares the constructed control signals obtained from our simulations qualitatively.

II. Listing's and Donders' Constraints

We assume a global coordinate system, shown in Fig. 1(b), fixed with respect to the torso and that the head and the eye rotate about the center of this system.[7] Furthermore, assume that the head and the eye orientations are observed with respect to this coordinate system and that every orientation is a point in $\mathbf{SO(3)}$. Without any loss of generality, the head is assumed to be initially located at the identity matrix $\mathbf{I}$. Following [13] and [14], we describe an axis angle coordinate system on $\mathbf{SO(3)}$ using a coordinate map on $\mathbf{S}^3$ as follows:

$$\rho \ : \ [0, 2\pi\,] \times [0, \pi\,] \times \left[-\frac{\pi}{2}, \frac{\pi}{2}\right] \rightarrow S^3 \tag{1}$$

where

$$\rho(\theta, \phi, \alpha) = \left(\cos\tfrac{\phi}{2},\ \sin\tfrac{\phi}{2}\cos\theta\ \cos\alpha,\ \sin\tfrac{\phi}{2}\sin\theta\cos\alpha,\ \sin\tfrac{\phi}{2}\sin\alpha\right)^T. \tag{2}$$

It is *a priori* unclear why one chooses the angle parameters as in (2). To see the connection between the chosen parameters of $\mathbf{S}^3$ and $\mathbf{SO(3)}$, we consider the map rot from [14], given by

$$\text{rot} \ : \ \mathbf{S}^3 \rightarrow \mathbf{SO(3)}. \tag{3}$$

The image of the composite map $\text{rot} \circ \rho(\theta, \phi, \alpha)$ is a rotation matrix [13], which rotates a vector in $\mathbf{R}^3$ around the axis[8]

$$\tan\frac{\phi}{2}\ (\cos\theta\ \cos\alpha,\ \ \sin\theta\ \cos\alpha,\ \ \sin\alpha)^T \tag{4}$$

by a counterclockwise angle ϕ. Every point of $\mathbf{S}^3$ is considered as a unit quaternion [15].[9] The map **rot** is a $2-1$ map and every unit quaternion q and $-q$ are mapped to the same rotation matrix in $\mathbf{SO(3)}$. The angle parameter vector (θ, ϕ, α) can therefore be viewed as a coordinate on $\mathbf{SO(3)}$. The vector (4) is called the rotational vector (see footnote 1). Note that the scaler $\tan\phi/2$ is the magnitude of the rotational vector.

Donders' law states that for head rotation, the rotational vectors (4) lie in a surface that goes by the name Donders' surface [13]. One way to describe this surface, is to write the torsion angle parameter α as a function of the other two parameters θ and ϕ. Another way is to describe the surface using the quaternion coordinates of $\mathbf{S}^3$. When the torsion is zero, i.e., when $\alpha = 0$, the Donders' surface reduces to a plane that goes by the name Listing's plane [14]. The Donders' surface, in general, is not fixed but changes from one human subject to another. For example, for the six subjects considered in this brief, the corresponding Donders' surfaces are computed from the observed head orientation data, as described in [10]. We now proceed to describe how the eye fixates on a stationary point target in space, while both the head and the eye are free to move, without any *a priori* restriction on their axes of rotation.

When a point target is introduced in the visual space, eye rotates to fixate on the target as quickly as possible. We assume that this motion takes place in $\mathbf{S}^3$, since this particular eye motion does not satisfy Listing's constraint. Let $e = [e_0, e_1, e_2, e_3]^T$ be the coordinates (unit quaternion coordinates) of the target with respect to a fixed global coordinate system (assumed attached to the torso

[5]For all the simulations presented in this brief, the fixed time interval is chosen to be [0, 1]. The actual time intervals of the trajectories have not been used.

[6]Although the objective of this brief is to fixate the eye onto a stationary target, eye tracking is required to compensate for the moving head.

[7]The eye movements can additionally be described with respect to the moving frame shown in Fig. 1(a). This description is particularly useful when we describe the Listing's plane.

[8]The three coordinates of this axis are the x, y, and z coordinates in Fig. 1.

[9]The quaternion structure of S^3 will be explored later in this section.

in this brief).[10] Furthermore, we assume that $m(t) = [m_0(t), m_1(t), m_2(t), m_3(t)]^T$ are the unit quaternion coordinates of the moving head, with respect to the same global coordinate system. It follows that the coordinates of the target, with respect to a coordinate system attached to the head, is given by $\xi(t) = m(t)^{-1} \cdot e$, where $\cdot$ is the symbol used for quaternion multiplication (see [16] for a definition). Finally, we assume that at $t = 1$, the head comes to a stop. We would like to choose the orientation component of e in such a way that $\xi(1)$ satisfies Listing's constraint.

The following Lemma describes the constraint between $m(1)$ and e dictated by the Listing's constraint.

Lemma I: A necessary and sufficient condition for $\xi(1)$ to satisfy Listing's constraint is given by

$$e_0 m_3(1) + e_2 m_1(1) = e_1 m_2(1) + e_3 m_0(1). \tag{5}$$

Proof of Lemma I: The unit quaternion coordinates of the target with respect to the moving head coordinates is given by

$$[m_0(t), -m_1(t), -m_2(t), -m_3(t)] \cdot [e_0, e_1, e_2, e_3]. \tag{6}$$

In order for the Listing's constraint to be satisfied, the last coordinate of the product in (6) must be zero at $t = 1$. The condition (5) easily follows. □

Although the quaternion e is not completely specified by the direction of the point target, the imposed Listing's constraint uniquely specifies the vector $\xi(1)$. The vector e can now be uniquely obtained as $e = m(1) \cdot \xi(1)$. Consequently, the target coordinate vector $\xi(t)$, in the moving head coordinates, can be written as

$$\xi(t) = m(t)^{-1} \cdot m(1) \cdot \xi(1). \tag{7}$$

Remark I: The signal $\xi(t)$ is completely described using the head trajectory $m(t)$, the final head orientation $m(1)$, and $\xi(1)$ obtained from the direction of the fixed point target together with the Listing's constraint. We conjecture that the eye control system tracks the signal $\xi(t)$. This will result in the eye gazing the target with unchanged orientation in the global torso coordinates and the eye orientation satisfying the Listing's constraint at $t = 1$. Of course, at all time t, the head coordinates satisfy an additional constraint imposed by Donders' law. In this brief, we assume that the Donders' surface is quadratic and is of the form

$$\begin{aligned} m_3 m_0 = {} & h_0 m_0^2 + 2h_1 m_1 m_0 + 2h_2 m_2 m_0 + h_{11} m_1^2 + h_{22} m_2^2 \\ & + 2h_{12} m_1 m_2 \end{aligned} \tag{8}$$

where the parameters h_* have been precomputed and are assumed known. The Donders' surface parameters are computed for six subjects and reported in [10]. □

Remark II: Computation of $m(1)$ and subsequently $\xi(1)$ would require that the final orientation of the head is known ahead of time by the eye controller. The computation of the tracking signal $\xi(t)$ would additionally require knowledge of 3-D location of the point target, and the instantaneous head orientation $m(t)$, assumed to be part of a feed forward coupling between the head and the eye system. How the eye controller anticipates the head position is unclear. □

[10]It is assumed that the target is a point. It would follow that the target direction, corresponding to the last column of rot(e), is completely specified by the target direction. Orientation component of e is still ambiguous at this stage.

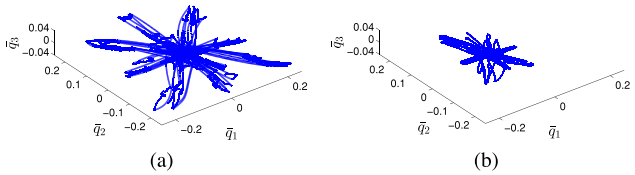

Fig. 2. Typical eye and head movement manoeuvres for one of the six human subjects considered in this brief. The movements are plotted in the same scale showing that the head movements are smaller than the eye movements. (a) Experimentally recorded eye trajectory in head coordinates. (b) Experimentally recorded head trajectory in torso coordinates.

Remark III: Eye movement data [Fig. 2(a)] has been recorded in conjunction with head movement [Fig. 2(b)] from six subjects, aged 25–38 years with no known neurological or orthopedic disorders. For 3-D eye movement recordings, a dual search coil was used on the left eye (Skalar, Delft, The Netherlands) and for the 3-D head movements, two coils mounted on a head ring at 90° angle between them was used. Both head and eye coils measured absolute position in the space. Therefore, when the head was allowed to move, the eye coil recorded gaze (combined eye and head) movements. The subjects were seated in complete darkness inside a magnetic field and were instructed to follow a laser dot. Subjects had to follow the target with a combination of natural eye and head movements. The laser dot jumped randomly between the center and eight peripheral positions, so that each final position is reached from a different initial position (see Fig. 2 for the laser dot movements corresponding to the eye and the head). For complete details, we would refer to [17] and [18]. For the head and the eye movement data from six subjects, we display in Table I (left) the extent to which Donders' law is satisfied by the actual head movement trajectories [see the first column of Table I (left)], and in Table I (right) the extent to which Listing's law is satisfied by the final eye orientation [see the first column of Table I (right)], when the subject has fixated on the target and the eye and the head have come to rest. The point of showing the two tables is to emphasize that the two physiological constraints stemming from Donders and Listing are closely supported by observed data.[11] □

III. Head/Eye Movement Dynamics

The head and the eye movement trajectories are simulated using a dynamical system, constructed from an appropriate Lagrangian formulation, the main ideas of which are already sketched in [13] and [14]. We rewrite the main steps using coordinates (θ, ϕ, α) from Section II. Let $\rho(\theta, \phi, \alpha)$ be a parametrization of the manifold $\mathbf{S}^3$ as in (2). A Riemannian metric on $\mathbf{S}^3$ can be written using the matrix given by

$$G = \begin{pmatrix} \rho_\theta \cdot \rho_\theta & \rho_\theta \cdot \rho_\phi & \rho_\theta \cdot \rho_\alpha \\ \rho_\phi \cdot \rho_\theta & \rho_\phi \cdot \rho_\phi & \rho_\phi \cdot \rho_\alpha \\ \rho_\alpha \cdot \rho_\theta & \rho_\alpha \cdot \rho_\phi & \rho_\alpha \cdot \rho_\alpha \end{pmatrix} \tag{9}$$

[11]In the other columns of the two tables, we show that for the optimal and the potential controllers that we have implemented later in this brief, the Donders' and the Listing's constraints are closely enforced.

TABLE I

LEFT: FOR EACH SUBJECT, MAXIMUM ABSOLUTE VALUE OF THE DONDERS' ERROR, IN RADIANS, ARE DISPLAYED BY TAKING AVERAGE OVER ALL THE HEAD TRAJECTORIES. RIGHT: FOR EACH SUBJECT, ABSOLUTE VALUE OF THE FINAL LISTING'S ERROR, IN RADIANS, ARE DISPLAYED BY TAKING AVERAGE OVER ALL THE EYE TRAJECTORIES

subjects	actual	optimal	potential
1	0.0226	0.0000	0.0001
2	0.0177	0.0000	0.0002
3	0.0217	0.0000	0.0010
4	0.0150	0.0000	0.0008
5	0.0270	0.0000	0.0001
6	0.0093	0.0000	0.0000

subjects	actual	optimal	potential
1	0.0826	0.0000	0.0007
2	0.0200	0.0000	0.0003
3	0.0497	0.0000	0.0010
4	0.0533	0.0000	0.0012
5	0.0478	0.0000	0.0006
6	0.0366	0.0000	0.0001

where $\rho_\gamma = \partial\rho/\partial\gamma$ and dot in (9) is the vector dot product. Let us define $X = (\theta, \phi, \alpha)^T$ to be the vector of angle variables. As in [14], we define the kinetic energy[12] KE as

$$\text{KE} = \frac{1}{2}\dot{X}^T G \dot{X}. \tag{10}$$

If the potential energy is represented by V, the Lagrangian of the head movement system can be written as

$$L = \text{KE} - V. \tag{11}$$

The equation of motion on the Donders' surface, using the Euler Lagrange equation can now be described as

$$\frac{d}{dt}\frac{\partial L}{\partial \dot{\gamma}} - \frac{\partial L}{\partial \gamma} = \tau_\gamma \tag{12}$$

where γ can be the angle variable θ, ϕ, or α and where τ_γ is the generalized torque input (to be viewed as the control input) to the system. The resulting equations of motion can be expressed as

$$G\ddot{X} + \dot{G}\dot{X} - \frac{1}{2}\dot{X}^T \nabla_X G\, \dot{X} + \nabla_X V = \Gamma \tag{13}$$

where $\Gamma = (\tau_\theta \quad \tau_\phi \quad \tau_\alpha)^T$ and where ∇_X is the gradient operator with respect to X defined as

$$\nabla_X = \left(\frac{\partial}{\partial\theta}, \frac{\partial}{\partial\phi}, \frac{\partial}{\partial\alpha}\right). \tag{14}$$

Remark IV: In this brief, the potential energy term V is assumed to be identically zero, when we are looking at optimal control problems. On the other hand, when the control is potentially driven, the potential energy term V is present. We also add a suitable damping term to the equations of motion (13), to asymptotically stabilize the state vector around the point where V is minimum. □

IV. TRACKING AND OPTIMAL ROTATION OF HUMAN HEAD AND EYE

We begin this section recalling from Remark I that, in order for the eye orientations to satisfy Listing's constraint when the head and the eye comes to a stop, while the eye is gazing at the target in spite of prior head movements, the eye has to track a trajectory $\xi(t)$. We now describe three simulation scenarios, already introduced in Section I.

A. Simulation I: Head and Eye Tracking an Observed Trajectory (Optimal Tracking Strategy)

Assume that the dynamics of the head or eye is given by[13]

$$G\ddot{X} + \dot{G}\dot{X} - \frac{1}{2}\dot{X}^T \nabla_X G\, \dot{X} = \Gamma. \tag{15}$$

We would like to rewrite the dynamics (15) as

$$\ddot{X} + G^{-1}\dot{G}\dot{X} - \frac{1}{2}G^{-1}\dot{X}^T \nabla_X G\, \dot{X} = \Gamma_1 \tag{16}$$

where

$$\Gamma_1 = G^{-1}\Gamma. \tag{17}$$

For both, the head and the eye, we consider a cost function given by

$$J = \int_0^1 \frac{\delta}{2}\Gamma_1^T\Gamma_1 + \frac{\beta}{2}C^T C + p^T\left(F - \ddot{X}\right)\, dt \tag{18}$$

where $\ddot{X} = F$ is the motion dynamics (16), $C = (A(t) - X)$ and $A(t)$ is the trajectory to track.[14] The function $p(t)$ is the Lagrange multiplier. The trajectory $A(t)$ has been obtained from observed head and eye trajectory data. The parameters for the cost function (18) are chosen as follows: $\delta = 2$, $\beta = 2\times10^6$ (for the head and the eye dynamics). An artificially high value of β is chosen to obtain a near perfect tracking. The initial and final orientations of the head and the eye are chosen to match the corresponding observed orientations. Boundary conditions are prescribed by choosing the vector $(X(0), \dot{X}(0), X(1), \dot{X}(1))$.

Remark V: Instead of using the generalized torque vector Γ in the cost function (18), we have chosen Γ_1, which is obtained by scaling Γ by the matrix G. We would like to remark that the optimal control problem (16) and (18) is scale invariant, in the sense that if G is scaled by a constant scale factor υ, the control Γ is likewise scaled, while the dynamics (16) and the cost function (18) remain unaltered. Hence, the relative weights of control energy and tracking error in the cost function (18) does not change. The model can therefore be used for both, the eye and the head, which differ from each other by a scale factor in G, referred to in footnote 12. □

Remark VI: It is possible to replace the vector Γ_1 by a physically meaningful externally applied resultant torque vector T in the cost function (18), as has been suggested in [19]. One can show [9], that

$$\|T\|^2 = \frac{1}{4}\Gamma_1^T G \Gamma_1. \qquad \square$$

The Hamiltonian [14] for this problem is defined as

$$H = \frac{\delta}{2}\Gamma_1^T\Gamma_1 + \frac{\beta}{2}C^T C + p^T F. \tag{19}$$

[12] Up to a scale factor, the kinetic energy has the form (10) for both the eye and the head.

[13] The model (15) can be used interchangeably for the eye or head. For the eye/head complex, two copies of this model is used.

[14] The term $C^T C$ in the cost function forces the state X to track the signal $A(t)$.

Using this notation, we write

$$J = \int_0^1 \left[H - p^T \ddot{X} \right] dt. \tag{20}$$

Applying the principle of variation, we obtain the following set of Hamilton's equations:

$$\ddot{X} = \frac{\partial H}{\partial p} = F; \quad \ddot{p} = \frac{\partial H}{\partial X} - \frac{d}{dt}\left(\frac{\partial H}{\partial \dot{X}}\right); \quad \Gamma_1 = -\frac{1}{\delta} p \tag{21}$$

where Γ_1 is obtained by setting $\partial H / \partial \Gamma_1 = 0$ and the optimal generalized torque control Γ is obtained from (17) as

$$\Gamma = -\frac{1}{\delta} G p. \tag{22}$$

Remark VII: In our data collection experiments, the eye and the head trajectories are observed, but the torque inputs are not observed. Via this simulation, we synthesize the control input using our dynamic model, that closely tracks the observed trajectories. Using the eye and the head movement trajectories, obtained in Simulation I, we presented in Fig. 3(a) the eye tracking error and in Fig. 3(d) the error between current and final position of the head, from observed data.[15] □.

B. Simulation II: Head and Eye are Optimally Controlled, Eye Reverse Tracking the Head Movement

As in Simulation I, we continue to assume that the dynamics of the head and the eye are given by (16). The cost function for the head is given by

$$J_H = \int_0^1 \frac{\delta}{2} \Gamma_1^T \Gamma_1 + p^T \left(F - \ddot{X} \right) + \lambda^T D + \frac{1}{2} \dot{\lambda}^T \epsilon \, \dot{\lambda} \, dt \tag{23}$$

and for the eye is given by

$$J_E = \int_0^1 \frac{\delta}{2} \Gamma_1^T \Gamma_1 + \frac{\beta}{2} C^T C + p^T \left(F - \ddot{X} \right) dt. \tag{24}$$

The cost function J_H is chosen so that the head is optimally controlled between two boundary points. It has four parts. The first part is a quadratic cost function on the control. The second part contains $\ddot{X} = F$ from the equations of motion (16), where $p(t)$ is the Lagrange multiplier. The third part constrains the state X onto the Donders' surface $D(X) = 0$ with a Lagrange multiplier λ. Finally, the fourth term is to be viewed as a penalty term, where the parameter ϵ decides on the level of smoothness of the Lagrange multiplier. The cost function J_E is chosen so that the eye optimally tracks a signal $A(t)$. The function has three parts, the first and the third are identical to J_H. The second part, where $C = (A(t) - X)$, constrains the state X to track the signal $A(t)$.[16] The parameters for the cost functions (23) and (24) are chosen as follows: $\delta = 2$, $\epsilon = 2 \times 10^{-8}$ (for the head dynamics); $\delta = 2$, $\beta = 20\,000$ (for the eye dynamics). Note that for the eye dynamics, the ratio of δ and β emphasizes the relative importance between the tracking error in comparison with the magnitude of the generalized torque. The chosen values force low-tracking error at a possibly higher magnitude of the generalized torque.

[15]The errors cannot be plotted directly from the data. This is because the observed data needs to be interpolated by a smoothing function. Simulation I has also been used for this purpose.

[16]The tracking function $A(t)$ is $\rho^{-1}\xi(t)$, where $\xi(t)$ is the tracking function (7) and ρ is the map defined in (1). $A(t)$ is thus the tracking function described in the angle coordinates θ, ϕ, α.

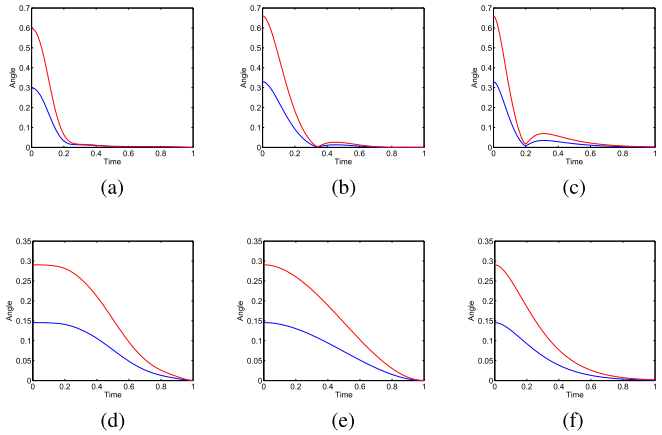

Fig. 3. (a) Eye tracking error when the head and eye are following observed trajectories from a human subject (Simulation I). (b) Eye tracking error when the head is following optimal trajectory on the Donders' surface with constrained initial and final points (Simulation II). (c) Eye tracking error when the head is potentially controlled toward a final point and is constrained by the Donders' surface (Simulation III). (d) Head is following observed trajectory from a human subject (Simulation I). (e) Head is following optimal trajectory constrained by the Donders' surface with fixed initial and final conditions (Simulation II). (f) Head follows a path of decreasing potential function toward a final point and is constrained by the Donders' surface (Simulation III). Top: eye tracking error, in torso coordinates, has been expressed as angles. Blue: angle between the eye quaternion and the target represented as a quaternion. Red: angle between the eye direction and the target direction. Bottom: error between current and final position of the head, in torso coordinates, has been expressed as angles. Blue: angle between the current head quaternion and the final head quaternion. Red: angle between the current head direction and the final head direction.

The initial and final orientations of the head and the eye are chosen as follows. For the head, the observed orientations at the end points are projected onto the Donders' surface. The projected end points are chosen as the boundary conditions for our simulation. For the eye, the initial orientation coincides with the straight gaze direction, i.e., the eye looking straight with respect to the head coordinates. The final orientation of the eye satisfies Listing's constraint with respect to the final orientation of the head, while gazing directly at the target. Boundary conditions are prescribed by choosing the vector $(X(0), \dot{X}(0), X(1), \dot{X}(1))$.

The Hamiltonian [14] for the head is defined as

$$H_H = \frac{\delta}{2} \Gamma_1^T \Gamma_1 + p^T F + \lambda^T D \tag{25}$$

and we write

$$J_H = \int_0^1 \left[H_H - p^T \ddot{X} + \frac{1}{2} \dot{\lambda}^T \epsilon \, \dot{\lambda} \right] dt. \tag{26}$$

Applying the principle of variation, we obtain the following set of Hamilton's equations:

$$\ddot{X} = \frac{\partial H_H}{\partial p} = F; \quad \ddot{p} = \frac{\partial H_H}{\partial X} - \frac{d}{dt}\left(\frac{\partial H_H}{\partial \dot{X}}\right)$$
$$\ddot{\lambda} = \epsilon^{-1} \frac{\partial H_H}{\partial \lambda}; \quad \Gamma_1 = -\frac{1}{\delta} p \tag{27}$$

where the optimal control Γ_1 is obtained by setting $\partial H_H / \partial \Gamma_1 = 0$. As before, the control Γ is given by (22). The Hamiltonian [14] for the eye is same as (19) and the corresponding Hamilton's equations are given by (21). Finally, the optimal control Γ is given by (22).

Remark VIII: To solve the two point boundary value problems of the kind introduced in (21) and (27), we discretize the equations using Comsol-Multiphysics finite element software [20], widely used in the computational community to solve both initial and boundary value problems. The software automatically generates Galerkin finite element approximation [21] for a specific PDE equation, once the problem is entered in its weak or strong formulation. The Comsol software facilitates the solution of multiphysics nonlinear coupled problem, where the Jacobian in the Newton iteration scheme is evaluated through automatic differentiation [22]. The corresponding linearized system is then solved using a direct or iterative solver. □

V. Tracking With Potential Control in Human Head and Eye

Instead of minimizing a cost function (18), (23), and (24), we show in this section that the head and the eye rotations can be controlled using a potential function and an added damping term. The potential function is described [10] as follows:

$$V(\theta, \phi, \alpha) \;=\; A\,(1 - |\rho(\theta, \phi, \alpha).\rho_0|) \tag{28}$$

where A is a constant parameter, ρ_0 is a fixed unit quaternion, and $\rho(\theta, \phi, \alpha)$. The ρ_0 represent the dot product of two vectors in $\mathbb{R}^4$. It can be observed that the minima occurs at $\rho = \rho_0$ or $\rho = -\rho_0$. Both of these minima correspond to a unique point on SO(3) via the map rot introduced in (3). The parameter ρ_0 can be constant or can vary in time.

A damping term is added externally using the generalized torque input Γ, the goal of which is to dampen the movement so that it comes to a rest at the desired pointing direction and orientation, described by ρ_0. We consider a damping term described by

$$\Gamma_1 \;=\; -c\,\dot{X} \tag{29}$$

where c is an arbitrary constant. The motion equation (13) is written as

$$\ddot{X} \;+\; (G^{-1}\dot{G} \;+\; c)\,\dot{X} \;-\; \frac{1}{2}G^{-1}\dot{X}^T\nabla_X G\,\dot{X} \\ +G^{-1}\nabla_X V \;=\; 0. \tag{30}$$

If we now define

$$\Gamma_2 \;=\; -c\dot{X} - G^{-1}\nabla_X V \tag{31}$$

we have an equation similar in form to (16), given by

$$\ddot{X} \;+\; G^{-1}\dot{G}\dot{X} \;-\; \frac{1}{2}G^{-1}\dot{X}^T\nabla_X G\,\dot{X} \;=\; \Gamma_2. \tag{32}$$

The generalized torque vector $\Gamma = G\Gamma_2 = -cG\dot{X} - \nabla_X V$ is called the potential control [10]. Note that the potential control is a combination of the damping term and the gradient of the potential function.

Remark IX: Similar to observation made in Remark V, we note that the motion equation (30) remains unchanged when G and V are both scaled by a fixed scale factor. Thus, the motion equation (30) can be used for both, the eye and the head, which only differ from each other by a scale factor in G.

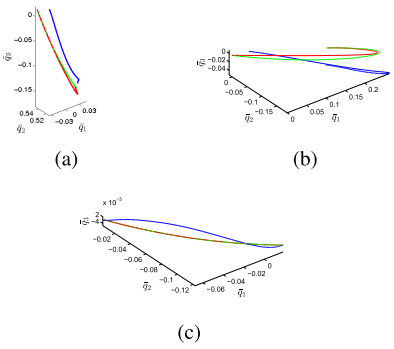

Fig. 4. (a) Eye movement trajectories with respect to the torso. (b) Eye movement trajectories with respect to the head. (c) Head movement trajectories with respect to the torso. Actual and simulated head and eye trajectories using scaled coordinates $\bar{q}_i = q_i/q_0$ for $i = 1, 2, 3$, where $[q_0, q_1, q_2, q_3]^T$ is the unit quaternion. These are coordinates of the rotational vector (4). Blue lines: actual trajectories. Red and green lines: trajectories from the Simulation II (optimal) and Simulation III (potential), respectively. Note that the head movement trajectories under the influence of optimal and potential control are surprisingly close, but differs from the actual trajectory. In addition, observe the backward movement of the eye in (b).

The two systems can, therefore be identically controlled by scaling V by the same scale factor. □

We now describe Simulation III in some details. As in Simulation II, the goal of the head control system is to drive the head from an initial orientation to a final orientation. However, as opposed to minimizing a cost function, the control drives the state toward smaller values of the potential function (28). We choose ρ_0 to coincide with the final orientation of the head. The goal of the eye controller is to track signal $A(t)$, which was introduced in Simulation II. To track a signal $A(t)$ using a potential function, we choose $\rho_0(t) = A(t)$ and the potential function is given by

$$V(\theta, \phi, \alpha, t) \;=\; A\,(1 - |\rho(\theta, \phi, \alpha) \cdot \rho_0(t)|). \tag{33}$$

It is easy to see that with the choice of the potential function (33), the orientation of the eye tracks the given target signal $A(t)$, provided that the constant A is chosen sufficiently large. In our simulation the parameters for the head system are chosen as $A = 40$, $c = 12$, and the parameters for the eye system are chosen as $A = 500$ and $c = 26$.

VI. Results

Recorded data from six subjects have been used to plot the head and the eye movement trajectories, when the head/eye complex has the task of acquiring a point target fixed in space with the eye starting from an initial primary position. The trajectories of the head and the eye are projected on the heading/gaze space and shown in the top three plots of Fig. 5. The trajectories are also shown in Fig. 4 on the coordinates of the rotational vector. In general, the eye trajectories are plotted with respect to, both, the fixed torso coordinates and the moving head coordinates. From the eye trajectories in Fig. 5, we infer that the effect of head movement is compensated by the back tracking movement of the eye. Fig. 4 is less informative but shows that the effect of optimal and potential control on the head trajectories, and to some extent on the eye trajectories, are surprisingly close. The simulated trajectories are somewhat

different from the actual trajectories observed and there are possibly two reasons for this. The first is that the Donders' and Listing's constraints are not tightly satisfied by the actual trajectory. This is evident from Table I (right), where we observe that the eye can deviate from the Listing's constraint by 2.77° on an average. Likewise, the head can deviate from the Donders' constraint by 1.082° on an average. The second is that the cost functions of the optimal controller and the potential functions considered in the potential controller need fine tuning. Such an inverse optimal/potential control problem has not been looked at, in this brief.

One of the key findings of this brief is evident in Fig. 5(a) and (d), where the eye trajectory using experimentally measured data is shown to track a computed trajectory (shown in black). This black trajectory is the tracking signal $\xi(t)$ in (7). In addition, we illustrate the point that the eye tracking is achieved in an optimal control setting by minimizing a cost function (24) and the optimal eye trajectory is shown in Fig. 5(b) with a closeup view in Fig. 5(e). The eye tracking is also achieved in a potential control setting by choosing a potential function (33) and the potential eye trajectory is shown in Fig. 5(c) with a closeup view in Fig. 5(f).

For each of the three simulations, the eye tracking error is shown in Fig. 3 (top). Error is displayed in blue by computing the angle between corresponding unit quaternion vectors and in red by computing the angle between unit gaze vectors. While looking at Fig. 3 (top), one would ask how quickly does the tracking errors go to zero and how stable is the error plot in the neighborhood of zero? From Fig. 3(c), it is evident that the potential eye trajectory goes to zero rapidly, but it overshoots immediately. On the other hand, we observe from Fig. 3(b) that the optimal eye trajectory goes to zero relatively slow. The tracking error for the observed eye trajectory, shown in Fig. 3(a), show that the error goes to zero rapidly as well, and is quite stable. Although, Fig. 3 (top) displays the error plot for one subject performing one manoeuvre, this picture has been averaged over multiples manoeuvres and six subjects. It has been observed that on an average, the potential eye trajectory goes to zero most rapidly, the optimal eye trajectory is most stable. The actual eye trajectories lie in between the optimal and the potential.

Head trajectories are simulated and studied in [10] and Fig. 3 (bottom) describes how rapidly does the head reaches its final end point. The figure displays similarity between the actual and the optimal trajectories in comparison with the actual and potential trajectories. Finally, in Figs. 6 and 7, the actual generalized torque input to the head/eye complex is compared with the simulated generalized torque inputs required for the optimal and the potential controller. In Figs. 6(a) and 7(a), the three components of the generalized torque inputs are plotted assuming that the head and the eye track an experimentally observed trajectory. Since the torque inputs are not measured, we use optimal tracking methods described in Simulation I to reconstruct the torques.

VII. Discussion

Recorded data shows that during the process of acquiring a point target, fixed in space, human head/eye synchronizes

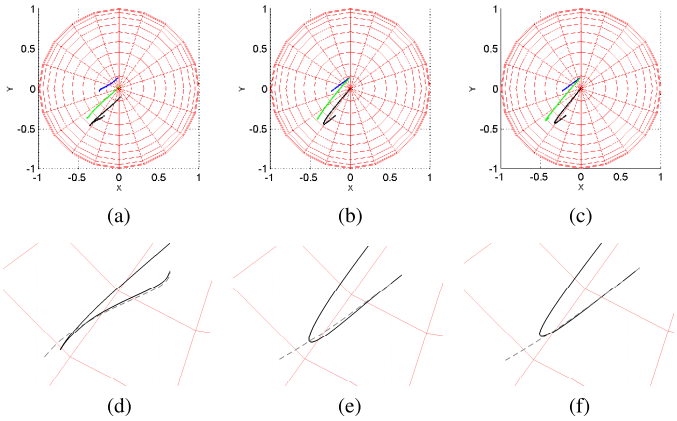

Fig. 5. (a) Actual trajectories of the head and eye using observed data from one human subject, performing one specific manoeuvre. (b) Head moves optimally satisfying boundary constraints, while the eye is backtracking the head movement (Simulation II). (c) Head moves potentially satisfying boundary constraints, while the eye is backtracking the head movement (Simulation III). (d) Closeup view of the bottom curve in (a). (e) Closeup view of the bottom curve in (b). (f) Closeup view of the bottom curve in (c). In (a)–(c), trajectories of the head and the eye are projected on the gaze (heading) space. All trajectories start near the center of the circle. Short (blue) trajectory on top is the head movement. Green trajectory in the middle is the eye movement with respect to a fixed global coordinate. Bottom (black) trajectory corresponds to the eye movement with respect to the moving head coordinates. All three black trajectories clearly show the backward movement of the eye corresponding to the forward movement of the head (see footnote 2). In (d)–(f), black curves are closeup views of the eye trajectories projected on the gaze space. Trajectories start at the top right corner of the figures. They move downward and reverses to follow a tracking signal. Dashed line is the tracking signal $\xi(t)$ (7) that the eye tracks.

their movements. To stabilize the image on the retina, the eye has to backtrack the forward movement of the head (see footnote 2). This keeps the eye fixed with respect to a global coordinate system. By constructing a dynamic model, we show in this brief that the backtracking movement of the eye can be reconstructed using two alternate forms of control strategy (optimal and potential), introduced earlier in [10], [13], and [14], for eye and head movement problems separately (see [9] for a survey). Eye and head movement data from six subjects have been analyzed in detail and the results are cumulated to derive conclusions reported in this brief. In addition, for the purpose of illustration, simulation results from one subject has been displayed in various figures presented.

In Fig. 5, the head and the eye trajectories have been displayed on the heading/gaze space. The actual and the simulated head/eye movements clearly show that the eye backtracks the forward movement of the head. In Fig. 4, the head and the eye trajectories are displayed on the rotational vector space. This figure illustrates the point that, as a trajectory there is a surprising closeness between the simulated trajectories under the two different control strategies. However, the simulated trajectories are far from the actual trajectory, indicating the fact that the control strategies require fine tuning.

One of the main result of this brief is shown in Fig. 5. In the beginning of this brief, we had conjectured that the eye has to track a computed tracking signal (in the head coordinate), based on the head movement and the 3-D location of the point target. This is required, in order for the head

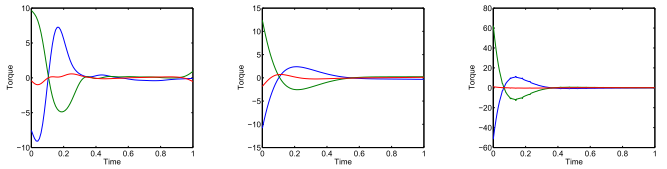

(a) (b) (c)

Fig. 6. Figures display three components of the generalized torques applied to the eye dynamics. (a) Head and eye are following an observed trajectory. (b) Head is following an optimal trajectory where the end points are constrained and the eye is backtracking the head. (c) Head is potentially controlled and the eye is backtracking the head. In (a), torque vector displayed is our estimate of the torque required for the eye dynamics to follow the observed trajectory. In (b) and (c), optimal and the potential torques are, respectively, displayed. All displayed torque vectors have been scaled, as defined by Γ_1 in (17).

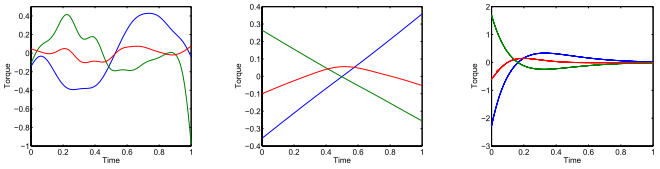

(a) (b) (c)

Fig. 7. Figures display three components of the generalized torques applied to the head dynamics. (a) Head and eye are following an observed trajectory. (b) Head is following an optimal trajectory where the end points are constrained and the eye is backtracking the head. (c) Head is potentially controlled and the eye is backtracking the head. In (a), torque vector displayed is our estimate of the torque required for the head dynamics to follow the observed trajectory. In (b) and (c), optimal and the potential torques are, respectively, displayed. All displayed torque vectors have been scaled, as defined by Γ_1 in (17).

and the eye to satisfy, respectively, the Donders' and Listing's constraints and for the image to be stabilized on the retina once the eye fixates on the target. The display on Fig. 5(d) shows the validity of this conjecture, by displaying the computed signal to be tracked (in dashed line). The actual eye movement trajectory (in black) shows the tracking movement of the eye. In Fig. 5(e) and (f), the tracking movements of the eye are displayed under optimal and potential controls, respectively. The tracking errors are displayed in Fig. 3 (top) and illustrate the point that the actual tracking errors drop to zero faster than the error under optimal control, and about the same time as the potential control. Unfortunately, the error under potential control, overshoots and settles down rather slowly. The error plots, between the current and the final head orientation, in Fig. 3 (bottom) show similarity between actual and the optimal head movements. Under potential control, the head moves rapidly in the beginning and slows down later, toward the end.

In Figs. 6 and 7, the generalized torque vectors are plotted for the head and the eye movements, respectively. We compute the generalized torques required for the actual head/eye movements to follow the observed trajectories. We compute the generalized torques required when the head/eye has to follow the optimal control strategy and the potential control strategy. As expected, the potential control takes higher values compared with the optimal control. For head movement control, closer to the end point, the potential control tapers off to zero, whereas the optimal control continues to maintain high values. The actual generalized torque, reconstructed from the data, does not taper off to zero for the head movement control, either. In this sense, the head movements are qualitatively similar to the optimal control strategy. All torques taper off to zero for the eye movement, but the torque profile for the optimal torque goes to zero slower in comparison with the actual torque and torque computed under potential control. Potential control and the actual control, both taper off to zero around the same time for eye movements, even though the potential control start from a higher magnitude. In this sense, the actual controls in eye movements are qualitatively similar to the controls obtained under the potential control strategy.

By and large, the potential controller is quick to fixate on the target. It is however, unable to retain the target stably. The optimal controller, on the other hand, is relatively slow in fixating on the target, but the target once acquired is retained well. The actual eye movements fall somewhere in between. For the parameters chosen in this brief, their ability to fixate on the target is never faster than the potential controller, and their ability to retain the target is always better than the optimal controller.

VIII. Additional Remarks and Notes on Controlling the Head/Eye Complex

It is well known [23] that eye movements are either reflexive or voluntary. The reflexive eye movements fall into the category of vestibulo-ocular reflex (VOR) and the optokinetic response. Voluntary eye movements, on the other hand could be saccadic or smooth-pursuit movements. This brief focuses on the VOR, to build a control strategy for eye movement to compensate for the moving head. Although the eye control signals are typically generated by the vestibular circuit [24], this circuit has not been modeled.

It has been recently observed [25], that the optimal eye control is generated not entirely at the vestibular level. It is proposed that an efference copy of the head movement is used to stabilize gaze and that cerebellum [26] plays a role in the process of generating the required motor commands.[17]

As pointed out in [25], there are many ways of combining eye and head movements to perform large gaze shifts. The very fact that an unique selection of movements are chosen [27] suggests some level of optimality (see [13], [14] for a discussion of optimal control for eye and head movements separately). For the combined head/eye complex, [12] has recently shown (in the context of horizontal eye and head movements), that movements are optimally selected to minimize gaze variability. This fact was also proposed earlier [28], [29] for head fixed saccades. This brief extends this line of research to 3-D, using geometric mechanics [30].[18] Optimal tracking control is introduced as one way to implement gaze stabilization. Implementation of this control at a vestibular and cerebellar level, with vestibular induced motor learning, has not been looked into.

[17] The vestibular circuit shapes the motor command, optimize gaze shifts and calibrate the head-movement efference copy, in the cerebellum, to stabilize gaze.

[18] 3-D head and eye movements with signal dependent noise is a subject of future research.

Remark X: Although targets are assumed to be stationary in this brief, our model head/eye complex can be controlled to follow a moving target as well. It is unclear, however, what would be the appropriate form of Listing's constraint, the eye would satisfy in this case.

IX. Conclusion

This brief extends our earlier study on head movement control problem [10] where, either the head movements are actuated by a controller, which minimizes a suitably chosen cost function (optimal control) or the control signals drive the head toward a path that reduces a suitably chosen potential function (potential control). We apply the optimal and potential control strategies to both the head and the eye movement problems. An important distinction between potential and optimal control strategies is that, potential controller drives the system-states rapidly in the beginning followed by small changes toward the end. On the other hand, an optimal controller drives the system-states somewhat evenly throughout the entire time of actuation. A consequence of this qualitative difference between a potential and an optimal controller is that, the applied torques during potential control are large initially and taper off to small values subsequently during actuation. On the other hand, the control torques during optimal control maintain large values, most of the time, during entire period of actuation. On the basis of the this criterion, we find that the actual head movement has the qualitative features of an optimal head movement. From the point of view of how rapidly the tracking error goes to zero and how stable the target is, once it is acquired, the actual eye movement falls somewhere in between optimal and the potential control schemes discussed in this brief.

References

[1] J. B. Listing, *Beiträge zur Physiologischen Optik*. Göttingen, Germany: Vandenhoeck und Ruprecht, 1845.

[2] F. C. Donders, "Beiträge zur Lehre von den Bewegungen des menschlichen Auges," *Holländische Beiträge Anatomischen Physiol. Wissenschaften*, vol. 1, pp. 104–145, 1848.

[3] H. von Helmholtz, *Handbuch der Physiologischen Optik*, 3rd ed., vol. 3. Hamburg, Germany: Leopold Voss, 1910.

[4] M. Ceylan, D. Y. P. Henriques, D. B. Tweed, and J. D. Crawford, "Task-dependent constraints in motor control: Pinhole goggles make the head move like an eye," *J. Neurosci.*, vol. 20, no. 7, pp. 2719–2730, Apr. 2000.

[5] D. Straumann, T. Haslwanter, M. C. Hepp-Reymond, and K. Hepp, "Listing's law for eye, head and arm movements and their synergistic control," *Experim. Brain Res.*, vol. 86, no. 1, pp. 209–215, 1991.

[6] B. Glenn and T. Vilis, "Violations of Listing's law after large eye and head gaze shifts," *J. Neurophysiol.*, vol. 68, no. 1, pp. 309–318, 1992.

[7] D. Tweed and T. Vilis, "Listing's law for gaze directing head movements," in *The Head-Neck Sensory Motor System*, A. Berthoz, W. Graf, and P. P. Vidal, Eds. New York, NY, USA: Oxford Univ. Press, 1992, pp. 387–391.

[8] D. Tweed, T. Haslwanter, and M. Fetter, "Optimizing gaze control in three dimensions," *Science*, vol. 281, no. 5381, pp. 1363–1365, Aug. 1998.

[9] B. K. Ghosh, I. B. Wijayasinghe, and S. D. Kahagalage. (2014). "A geometric approach to head/eye control," vol. 2, pp. 316-–332. [Online]. Available: dx.doi.org/10.1109/ACCESS.2014.2315523

[10] I. Wijayasinghe *et al.* (2013). Potential and optimal control of human head movement using Tait-Bryan parametrization. *Automatica* [Online]. Available: http://dx.doi.org/10.1016/j.automatica.2013.11.017

[11] A. A. Kardamakis and A. K. Moschovakis, "Optimal control of gaze shifts," *J. Neurosci.*, vol. 29, no. 24, pp. 7723–7730, 2009.

[12] M. Sağlam, N. Lehnen, and S. Glasauer, "Optimal control of natural eye-head movements minimizes the impact of noise," *J. Neurosci.*, vol. 31, no. 45, pp. 16185–16193, 2011.

[13] B. K. Ghosh and I. B. Wijayasinghe, "Dynamics of human head and eye rotations under Donders' constraint," *IEEE Trans. Autom. Control*, vol. 57, no. 10, pp. 2478–2489, Oct. 2012.

[14] A. D. Polpitiya, W. P. Dayawansa, C. F. Martin, and B. K. Ghosh, "Geometry and control of human eye movements," *IEEE Trans. Autom. Control*, vol. 52, no. 2, pp. 170–180, Feb. 2007.

[15] S. W. Sheppard, "Quaternion from rotation matrix," *J. Guid. Control*, vol. 1, no. 3, pp. 223–224, May/Jun. 1978.

[16] S. L. Altmann, *Rotations, Quaternions, and Double Groups*. London, U.K.: Oxford Univ. Press, 1986.

[17] S. Glasauer, M. Hoshi, U. Kempermann, T. Eggert, and U. Büttner, "Three-dimensional eye position and slow phase velocity in humans with downbeat nystagmus," *J. Neurophysiol.*, vol. 89, no. 1, pp. 338–354, 2003.

[18] O. Kremmyda, S. Glasauer, L. Guerrasio, and U. Büttner, "Effects of unilateral midbrain lesions on gaze (eye and head) movements," *Ann. New York Acad. Sci.*, vol. 1233, no. 1, pp. 71–77, 2011.

[19] A. M. Bloch, I. I. Hussein, M. Leok, and A. K. Sanyal, "Geometric structure-preserving optimal control of a rigid body," *J. Dyn. Control Syst.*, vol. 15, no. 3, pp. 307–330, 2009.

[20] W. B. J. Zimmerman, *Multiphysics Modelling with Finite Element Methods*. Singapore: World Scientific, 2006.

[21] S. C. Brenner and L. R. Scott, *The Mathematical Theory of Finite Element Methods*, 3rd ed. New York, NY, USA: Springer-Verlag, 2008.

[22] A. Griewank and A. Walther, *Evaluating Derivatives: Principles and Techniques of Algorithmic Differentiation*, 2nd ed. Philadelphia, PA, USA: SIAM, 2008.

[23] M. Ito, *The Cerebellum and Neural Control*. New York, NY, USA: Raven, 1984.

[24] M. Ito, "Cerebellar control of the vestibulo-ocular reflex—Around the flocculus hypothesis," *Ann. Rev. Neurosci.*, vol. 5, no. 1, pp. 275–296, 1982.

[25] M. Sağlam, S. Glasauer, and N. Lehnen, "Vestibular and cerebellar contribution to gaze optimality," *Brain*, vol. 137, no. 4, pp. 1080–1094, 2014.

[26] A. J. Bastian, "Learning to predict the future: The cerebellum adapts feedforward movement control," *Current Opinion Neurobiol.*, vol. 16, no. 6, pp. 645–649, 2006.

[27] D. Guitton and M. Volle, "Gaze control in humans: Eye-head coordination during orienting movements to targets within and beyond the oculomotor range," *J. Neurophysiol.*, vol. 58, no. 3, pp. 427–459, 1987.

[28] C. M. Harris and D. M. Wolpert, "Signal-dependent noise determines motor planning," *Nature*, vol. 394, no. 6695, pp. 780–784, 1998.

[29] R. J. van Beers, "The sources of variability in saccadic eye movements," *J. Neurosci.*, vol. 27, no. 33, pp. 8757–8770, 2007.

[30] R. Abraham and J. E. Marsden, *Foundations of Mechanics*. Providence, RI, USA: AMS, 1978.